Mon. Not. R. Astron. Soc. **363,** 954–966 (2005) doi:10.1111/j.1365-2966.2005.09494.x

Klein–Nishina effects in the spectra of non-thermal sources immersed in external radiation fields

Rafał Moderski,[1⋆] Marek Sikora,[1] Paolo S. Coppi[2,3,4] and Felix Aharonian[3]

[1] *Nicolaus Copernicus Astronomical Centre, Bartycka 18, 00-716 Warsaw, Poland*
[2] *Yale University, New Haven, CT 06520-8101, USA*
[3] *Max-Planck-Institut für Kernphysik, Heidelberg, Germany*
[4] *Kavli Institute of Particle Astrophysics and Cosmology, Stanford University, Stanford, CA 94305, USA*

Accepted 2005 August 5. Received 2005 July 26; in original form 2005 April 19

ABSTRACT

We provide a systematic numerical and analytical study of Klein–Nishina (KN) effects in the spectrum produced by a steady-state, non-thermal source where rapidly accelerated electrons cool by emitting synchrotron radiation and Compton up-scattering ambient photons produced outside the source. We focus on the case where q, the ratio of the ambient radiation field to source magnetic field energy densities, significantly exceeds unity. We show that the KN reduction in the electron Compton cooling rate causes the steady-state electron spectrum to harden at energies $\gamma \gtrsim \gamma_{\rm KN}$, where $\gamma_{\rm KN} = 1/4\epsilon_0$ and $\epsilon_0 = h\nu_0/m_{\rm e}c^2$ is the characteristic ambient photon energy. This hardening becomes noticeable in the synchrotron radiation from electrons with energies as low as $0.1\gamma_{\rm KN}$ and changes the synchrotron spectral index relative to its Thomson limit value by as much as $\Delta\alpha \sim 0.75$ for $q \gg 1$. The source synchrotron spectrum thus shows a high-energy 'bump' or excess, even though the electron acceleration spectrum has no such excess. In contrast, the low-energy Compton gamma-ray spectrum shows little distortion because the electron hardening compensates for the KN decline in the scattering rate. For sufficiently high electron energies, however, Compton cooling becomes so inefficient that synchrotron cooling dominates – an effect omitted in most previous studies. The hardening of the electron distribution thus stops, leading to a rapid decline in Compton gamma-ray emission, i.e. a strong spectral break whose location does not depend on the maximum electron energy. This break can limit the importance of Compton gamma-ray pair production on ambient photons and implies that a source's synchrotron luminosity may exceed its Compton luminosity even though $q > 1$. We discuss the importance of these KN effects in blazars, micro-quasars and pulsar binaries.

Key words: MHD – radiation mechanisms: non-thermal – quasars: general.

1 INTRODUCTION

Probably because of the initially greater sensitivity of radio telescopes, studies of the emission from non-thermal sources, e.g. the powerful radio jets found in active galactic nuclei (AGNs), focused on synchrotron radiation from relativistic electrons moving in a magnetic field. It was quickly realized, however, that the same relativistic electrons would also Compton up-scatter any ambient low-energy photons to produce emission at much higher, e.g. X-ray and gamma-ray, energies. A classic discussion of the emission spectrum expected from a gas of relativistic electrons, where synchrotron radiation and Compton scattering are the dominant energy loss mechanisms, may be found, for example, in Felten & Morrison (1966). Several of the standard approximations still used today are presented there, e.g. the delta function approximation which provides a one-to-one relation between the energies of the electrons and the synchrotron and Compton up-scattered photons produced by them. Of particular interest, these authors note that the processes of Compton up-scattering in the Thomson regime and synchrotron radiation both lead to quasi-continuous electron energy losses that are proportional to the square of the electron Lorentz factor (this is, in fact, not a surprise given that synchrotron radiation may be viewed as the Compton up-scattering of virtual magnetic field photons; see Blumenthal & Gould 1970). This implies that the shape of the energy distribution of cooled electrons does not depend on which process dominates their cooling and that the ratio of the luminosities for the resulting Compton and synchrotron emission components simply goes as $L_{\rm C}/L_{\rm syn} = u_0/u_B$, where u_0 and u_B are, respectively, the (comoving) low-energy radiation and magnetic field energy densities inside the source. This is

⋆E-mail: moderski@camk.edu.pl

very useful to know, for example, because if one measures $L_{\rm C}$ and $L_{\rm syn}$ and knows u_0, e.g. if the relevant low-energy ambient photons are due to the cosmic microwave background (CMB), then one can immediately derive the magnetic field strength in the source. Also, the shapes of the synchrotron and Compton emission spectra will be similar, with the Compton spectrum simply shifted up in energy relative to the synchrotron one by the factor ϵ_0/ϵ_B where $\epsilon_B = B/B_{\rm cr}$, $B_{\rm cr} = 4.4 \times 10^{13}$ G, and $\epsilon_0 = h\nu_0/m_{\rm e}c^2$ is the typical ambient photon energy. For mono-energetic ambient photons, the spectral shapes are in fact identical except for the effects of self-absorption in the low-energy portion of the synchrotron spectrum.

It is important to remember, however, that all of these convenient rules of thumb, used in many interpretation papers, break down when the electrons are sufficiently energetic to scatter with ambient photons in the Klein–Nishina (KN) limit, i.e. when $\gamma > \gamma_{\rm KN} = 1/4\epsilon_0$ (e.g. Blumenthal & Gould 1970). In such a case, the relation between up-scattered and incident photon energy changes (the up-scattered photon cannot have more energy than the incident electron), electrons can lose most of their energy in a single scattering rather than cooling quasi-continuously as a result of many small energy losses, and to the extent that a cooling rate is relevant, the ratio of Compton to synchrotron energy losses is now a decreasing function of energy and is less than u_0/u_B. A careful re-examination of the implications of treating the Compton scattering process correctly in this limit is timely now that satellite and ground-based gamma-ray telescopes have shown many extragalactic and some galactic compact objects to be strong emitters of GeV and TeV radiation. If produced by Compton up-scattering, i.e. the inverse Compton (IC) process, then these gamma-rays likely result from scatterings in the KN regime, and we must be accordingly careful in the interpretation of the multiwavelength observations for these objects.

Some of the possible KN 'corrections' have already been discussed or are well known. An obvious limit is the case when the ambient (target) photon energy density in the source is small and the energy density ratio $q = u_0/u_B$ is thus $\ll 1$. In this case, synchrotron losses always dominate over Compton losses regardless of electron energy. If we have a source where electrons are rapidly accelerated to high energies and subsequently cool via radiative losses, then the steady-state spectrum of the source (assuming on-going acceleration) is determined solely by the magnetic field and the 'injection' energy spectrum of electrons produced by the rapid acceleration process. We can therefore consider the electron distribution to be fixed, e.g. a power law with $n_\gamma \propto \gamma^{-s}$, and we just need to carry out the relatively easy computation of the Compton spectrum up-scattered by such an electron power law. For simplicity, let us assume that the ambient radiation field is approximately mono-energetic, again with characteristic energy ϵ_0. In this case, the resulting Compton emissivity is approximately a broken power law, with the usual Thomson-limit result of $j_\epsilon \propto \epsilon^{-(s-1)/2}$ for $\epsilon \ll \epsilon_{\rm KN}$, and the extreme KN-limit result of $j_\epsilon \propto \epsilon^{-s}\,\log(\epsilon)$ for $\epsilon \gg \epsilon_{\rm KN}$ where $\epsilon_{\rm KN} = \gamma_{\rm KN}$ (see, for example, Aharonian & Atoyan 1981). In other words, the synchrotron spectrum is unchanged from a Thomson approximation calculation while the Compton spectrum shows a strong spectral break at $\epsilon \sim \epsilon_{\rm KN}$ with a change in spectral index $\Delta\alpha = (s+1)/2$. For $s \gtrsim 2$, which seems typical for the known very high-energy gamma-ray sources, $\Delta\alpha \gtrsim 1.5$, i.e. is large, and given the usually poor statistics at the highest energies, this spectral break can easily be misinterpreted as an exponential cut-off due to the maximum electron energy in the source.

A much less obvious but still important limit is the case $q \gg 1$. For u_0 sufficiently large, one can in principle go to the opposite limit and ignore the effects of synchrotron cooling, solving directly the kinetic equation for the evolution of electrons due to Compton scattering. The steady-state electron and up-scattered photon spectra obtained for continuous electron acceleration and complete electron cooling via Compton scattering are discussed in detail by Zdziarski (1989) (see also Zdziarski & Krolik 1993). The main conclusion is that the equilibrium electron distribution hardens for $\gamma > \gamma_{\rm KN}$ compared to the Thomson approximation result. This is because electron energy losses are relatively less efficient in the KN limit and electrons remain longer at higher energies. This hardening of the electron spectrum compensates the decreased efficiency of Compton up-scattering, and the resulting photon spectrum shows no 'KN break' at $\epsilon \sim \epsilon_{\rm IC,KN}$. Interestingly, for a rapid acceleration process that effectively injects electrons into the source with an energy distribution $Q(\gamma) \propto \gamma^{-p}$ with $p = 2$, the Compton emissivity is $j_\epsilon \propto \epsilon^{-2}$, i.e. exactly the answer that would have been obtained in the Thomson limit. Note, though, an important difference from the Thomson result is that the correctly computed spectrum always cuts off at $\epsilon \sim \gamma_{\rm max}$, the maximum electron Lorentz factor, and that this cut-off is independent of the target photon energy ϵ_0. Also, for $p \neq 2$, the Compton spectrum in the KN regime does not follow the slope of the spectrum in the Thomson regime, steepening slightly if $p > 2$, and hardening if $p < 2$.

The analysis just mentioned, however, does not include synchrotron losses and does not consider the synchrotron emission produced as a result of these losses. The condition $q \gg 1$, in fact, only guarantees that synchrotron losses are negligible for $\gamma < \gamma_{\rm KN}$. At higher energies, the Compton loss rate decreases due to KN effects and eventually synchrotron cooling always dominates. Thus, several effects that are potentially important for high-energy sources may pass unnoticed. First, the hardening of electron distribution in the KN regime leads to a hardening of co-spatially produced synchrotron radiation. Prior work which touches on this aspect includes the following. Dermer & Atoyan (2002) invoke KN effects to explain the production of X-rays in large-scale jets via synchrotron radiation. Ravasio et al. (2003) invoke KN effects to explain the soft X-ray excess over the power-law high-energy synchrotron tail. Kusunose, Takahara & Kato (2004) and Kusunose & Takahara (2005) study KN effects in the context of flat-spectrum radio quasars (FSRQs). Secondly, for sufficiently high electron energies, synchrotron losses dominate and the electron distribution 'saturates' to one with the same slope as in the Thomson regime, but with a normalization factor q times larger. This effect was included by Khangulian & Aharonian (2005) in their studies of outflows from compact objects in high-mass X-ray binary (HMXB) systems, but not by Kusunose & Takahara (2005), even though some of their calculations involve electron energies high enough for synchrotron losses to be important.

In this paper, we provide a systematic study of KN effects in steady-state sources with $q \gg 1$, covering all the effects mentioned above. We use accurate numerical techniques that solve the exact integro-differential equations for the steady-state photon and electron energy distributions. However, we also present approximations that allow us to follow the various effects analytically using simple algebraic functions. We focus our studies on the case where the ambient radiation field is dominated by external photon sources with mono-energetic or power-law spectra. The paper is organized as follows. In Section 2 we analyse IC electron energy losses in the KN regime and compare them with the corresponding synchrotron energy losses. In Section 3 we present general and approximate formulae for the IC emissivities for the cases of isotropic and beamed ambient radiation fields. The energy distribution of relativistic electrons in a steady-state source with continuous electron injection is

discussed in Section 4. The KN effects in the synchrotron and IC spectra produced by such a source are analysed in Section 5. Our results are discussed in the context of specific astrophysical sources in Section 6 and summarized in Section 7.

2 ELECTRON ENERGY LOSSES

2.1 Inverse Compton energy losses

The rate of IC energy losses of relativistic, isotropically distributed electrons is (see Appendix C)

$$|\dot{\gamma}|_{\rm IC} = \frac{4c\sigma_{\rm T}}{3m_{\rm e}c^2} u_0 \gamma^2 F_{\rm KN}, \tag{1}$$

where

$$F_{\rm KN} = \frac{1}{u_0} \int_{\epsilon_{0,\rm min}}^{\epsilon_{0,\rm max}} f_{\rm KN}(\tilde{b}) u_{\epsilon_0}\, {\rm d}\epsilon_0, \tag{2}$$

$u_0 = \int_{\epsilon_{0,\rm min}}^{\epsilon_{0,\rm max}} u_{\epsilon_0}\, {\rm d}\epsilon_0$ is the total energy density of the radiation field, u_{ε_0} is the energy distribution of the ambient photons, and we re-express the electron energy as $\tilde{b} = 4\gamma\epsilon_0$ noting $\tilde{b} = 1$ corresponds to the transition between the Thomson and KN scattering regimes. The function $f_{\rm KN}(\tilde{b})$ is given by equations (C5) and (C3) in Appendix C. For $\tilde{b} \ll 1$ (Thomson limit), $f_{\rm KN} \simeq 1$; for $\tilde{b} \gg 1$ (KN limit), $f_{\rm KN} \simeq [9/(2\tilde{b}^2)](\ln\tilde{b} - 11/6)$. For $b \lesssim 10^4$, $f_{\rm KN}(\tilde{b})$ can be approximated by

$$f_{\rm KN} \simeq \frac{1}{(1+\tilde{b})^{1.5}}. \tag{3}$$

To estimate the effects of having an extended target photon energy distribution, let us assume that u_{ε_0} is a power law $\propto\epsilon_0^{-\alpha}$ and that $b_{\rm max} = 4\epsilon_{0,\rm max}\gamma_{\rm max} < 10^4$, so we may use approximation (3). Then we may write

$$F_{\rm KN} \propto \int_{\epsilon_{0,\rm min}}^{\epsilon_{0,\rm KN}} \epsilon^{-\alpha_0}\, {\rm d}\epsilon_0 + \epsilon_{0,\rm KN}^{1.5} \int_{\epsilon_{0,\rm KN}}^{\epsilon_{0,\rm max}} \epsilon_0^{-\alpha_0-1.5}\, {\rm d}\epsilon_0, \tag{4}$$

where $\epsilon_{0,\rm KN} = 1/4\gamma$. KN effects become important and $F_{\rm KN} < 1$ for $\gamma > \gamma_{\rm KN} \equiv 1/(4\epsilon_{0,\rm max})$. For $\alpha_0 < -0.5$, Compton energy losses for electrons with $\gamma > \gamma_{\rm KN}$ are dominated by scatterings on photons with the highest energies, $\sim\epsilon_{0,\rm max}$. We may then treat the photon distribution as mono-energetic, with $F_{\rm KN} \simeq f_{\rm KN}(\tilde{b} = 4\gamma\epsilon_{0,\rm max})$. For $-0.5 < \alpha_0 < 1$, Compton losses are instead dominated by scattering on photons with energy $\sim\epsilon_{0,\rm KN}$. In this case, we may make the so-called 'Thomson-edge' or 'KN cut-off' approximation that

$$F_{\rm KN} \simeq \frac{\int_{\epsilon_{0,\rm min}}^{\epsilon_{0,\rm KN}} \epsilon_0^{-\alpha_0}\, {\rm d}\epsilon_0}{\int_{\epsilon_{0,\rm min}}^{\epsilon_{0,\rm max}} \epsilon_0^{-\alpha_0}\, {\rm d}\epsilon_0} \simeq (\epsilon_{0,\rm KN}/\epsilon_{0,\rm max})^{-\alpha_0+1} = b^{\alpha_0-1}, \tag{5}$$

if we rewrite the electron energy as $b = 4\epsilon_{0,\rm max}\gamma$ and have $\epsilon_{0,\rm min} \ll \epsilon_{0,\rm max}$. A useful approximation that extrapolates to the Thomson limit for $b \to 0$ and has good accuracy for $0 < \alpha_0 < 1$ is then given by

$$F_{\rm KN} \simeq \frac{1}{(1+b)^{1-\alpha_0}}. \tag{6}$$

If we instead have $\alpha_0 > 1$, the Compton losses of the electrons are dominated by scatterings on the lowest energy photons available, at $\sim\epsilon_{0,\rm min}$. We may then use the approximation, $F_{\rm KN} \simeq f_{\rm KN}(\tilde{b} = 4\gamma\epsilon_{0,\rm min})$. If we further have $4\gamma_{\rm max}\epsilon_{0,\rm min} < 1$, then in fact all scatterings are effectively in the Thomson regime even if higher-energy ambient photons are present and $b_{\rm max} > 1$. To gauge the accuracy of approximations (3) and (6), we compare in Fig. 1 the approximate values of $F_{\rm KN}(b)$ to the exact ones for three different ambient photon spectra: mono-energetic, and power laws with $\alpha_0 \equiv -{\rm d}\ln u_{\varepsilon_0}/{\rm d}\ln\varepsilon_0 = 0.0$ and 0.5. From a similar analysis to that for the power-law case, we can show that $F_{\rm KN}$ for a Planckian (thermal) distribution is well approximated by treating the Planckian as a mono-energetic photon distribution with energy 2.8 kT.

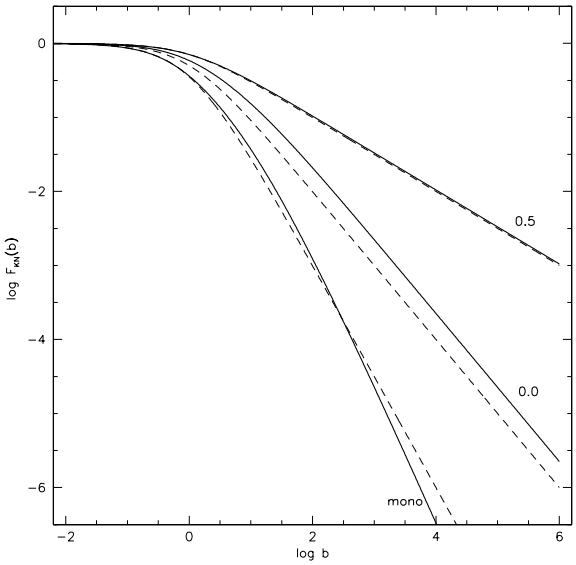

Figure 1. The function $F_{\rm KN}(b)$ computed for mono-energetic ('mono') and power-law ($\alpha_0 = 0.0$ and $\alpha_0 = 0.5$) energy distributions of the external photon field. The solid lines show the results of the exact calculations while the dashed lines are the analytical approximations.

2.2 Synchrotron energy losses versus inverse Compton energy losses

Noting that the rate of synchrotron losses in a tangled magnetic field of strength B is

$$|\dot{\gamma}|_{\rm syn} = \frac{4c\sigma_{\rm T}}{3m_{\rm e}c^2} u_B \gamma^2 \tag{7}$$

where $u_B = B^2/8\pi$ is the magnetic energy density, we have (see equation 1)

$$\frac{\dot{\gamma}_{\rm IC}}{\dot{\gamma}_{\rm syn}} = q F_{\rm KN}, \tag{8}$$

where $q \equiv u_0/u_B$. Because $F_{\rm KN} < 1$ for any value of b, for $q < 1$ the energy losses for all electrons are dominated by synchrotron radiation. For $q > 1$, the energy losses for electrons with $\gamma < \gamma_{\rm s}$ are dominated by IC scattering while losses for electrons with $\gamma > \gamma_{\rm s}$ are instead dominated by synchrotron radiation, where $\gamma_{\rm s} = b_{\rm s}/4\,\epsilon_{0,\rm max}$, and $b_{\rm s}$ is the solution of the equation $q F_{\rm KN} = 1$, plotted in Fig. 2. For a mono-energetic ambient photon spectrum (see equation 3)

$$b_{\rm s} \simeq q^{2/3} - 1, \tag{9}$$

while for a power-law spectrum with $0 < \alpha_0 < 1$ (see equation 6)

$$b_{\rm s} \simeq q^{1/(1-\alpha_0)} - 1. \tag{10}$$

The relative role of the IC and synchrotron energy losses is illustrated in Fig. 3. We show there

$$\frac{\dot{\gamma}_{\rm IC}}{\dot{\gamma}_{tot}} = \frac{q F_{\rm KN}(b)}{1 + q F_{\rm KN}(b)}, \tag{11}$$

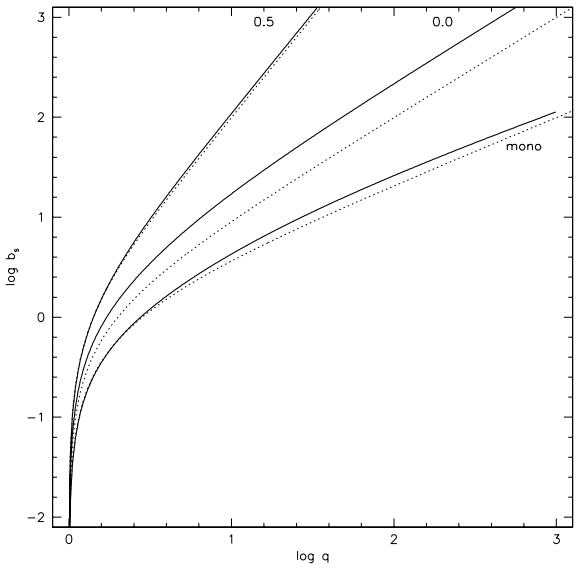

Figure 2. b_s versus q for mono-energetic and power-law ambient radiation fields: solid lines, exact results; dashed lines, analytical approximations.

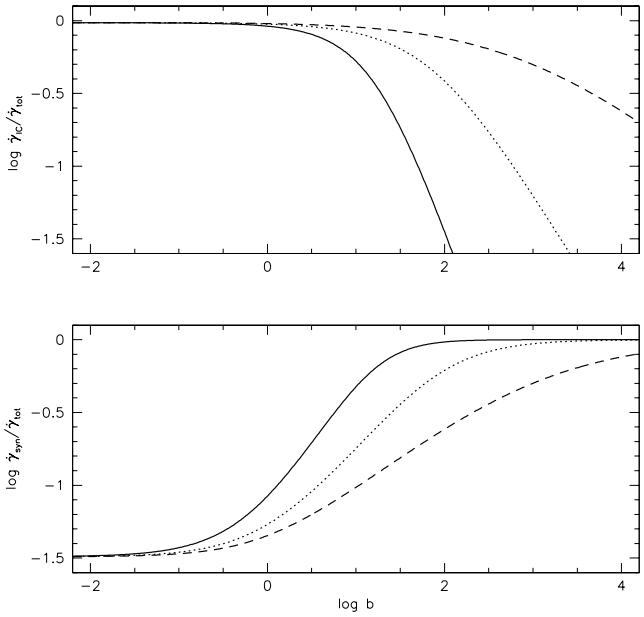

Figure 3. The relative IC and synchrotron energy losses for an ambient radiation energy distribution that is mono-energetic (solid lines) or power law ($\alpha_0 = 0.0$, dotted lines; $\alpha_0 = 0.5$, dashed lines).

and

$$\frac{\dot{\gamma}_{\rm syn}}{\dot{\gamma}_{\rm tot}} = \frac{1}{1 + q F_{\rm KN}(b)}, \tag{12}$$

for three different spectra of the ambient radiation field, assuming that $\dot{\gamma}_{\rm tot} = \dot{\gamma}_{\rm IC} + \dot{\gamma}_{\rm syn}$.

3 INVERSE COMPTON EMISSIVITY

The IC emissivity for isotropically distributed electrons is

$$j_{\epsilon({\rm IC})} = \int \frac{\partial P_{\epsilon({\rm IC})}(\gamma)}{\partial \Omega} n_\gamma \, {\rm d}\gamma, \tag{13}$$

where

$$\frac{\partial P_{\epsilon({\rm IC})}(\gamma)}{\partial \Omega} = \frac{\partial \dot{N}_{\rm sc}(\epsilon, \gamma)}{\partial \epsilon \partial \Omega} \epsilon m_{\rm e} c^2, \tag{14}$$

is the IC power per unit photon energy per unit solid angle per electron and $\dot{N}_{\rm sc}$ is the scattering rate of photons on isotropically distributed electrons.

For two particular cases, mono-directional beams of target photons and an isotropic radiation field, the respective scattering rates are given by equations (A1) and (B1), respectively. Inserting these into equation (13) gives, for the beamed mono-energetic external radiation field

$$\epsilon j_{\epsilon({\rm IC})}(\theta) = \frac{3}{16\pi} c \sigma_{\rm T} u_0 \left(\frac{\epsilon}{\epsilon_0}\right)^2 \int \frac{n_\gamma}{\gamma^2} f(\gamma, \epsilon, \epsilon_0, \theta) \, {\rm d}\gamma, \tag{15}$$

and for the isotropic ambient radiation field

$$\epsilon j_{\epsilon({\rm IC})} = \frac{3}{16\pi} c \sigma_{\rm T} u_0 \left(\frac{\epsilon}{\epsilon_0}\right)^2 \int \frac{n_\gamma}{\gamma^2} f_{\rm iso}(\gamma, \epsilon, \epsilon_0) \, {\rm d}\gamma, \tag{16}$$

where θ is the scattering angle (the angle between the photon beam and the direction to the observer). The functions $f(\gamma, \epsilon, \epsilon_0, \theta)$ and $f_{\rm iso}(\gamma, \epsilon, \epsilon_0)$ are given by equations (A3) and (B4). These formulae can easily be generalized for any spectrum of external radiation field by replacing u_0 by $u_{\varepsilon 0} \, {\rm d}\varepsilon_0$ and integrating them over ϵ_0.

A useful first approximation for the IC spectrum (see, for example, Coppi & Blandford 1990) may be obtained by making the delta function approximation $f(\epsilon, \gamma, \epsilon_0) \propto \delta[\epsilon - \bar{\epsilon}_{({\rm IC})}(\gamma)]$, where

$$\bar{\epsilon}_{\rm IC}(\gamma, \theta) = \frac{\int \epsilon f(\gamma, \epsilon, \epsilon_0, \theta) \, {\rm d}\epsilon}{\int f(\gamma, \epsilon, \epsilon_0, \theta) \, {\rm d}\epsilon} \tag{17}$$

$$\bar{\epsilon}_{\rm IC}(\gamma) = \frac{\int \epsilon f_{\rm iso}(\gamma, \epsilon, \epsilon_0) \, {\rm d}\epsilon}{\int f_{\rm iso}(\gamma, \epsilon, \epsilon_0) \, {\rm d}\epsilon} \tag{18}$$

are the average energies of photons produced by the scattering of photons of energy ϵ_0 by electrons with energy γ. A useful quantity is the scattering inelasticity of a single electron, i.e. the average fraction of its incident energy that is transferred to the scattered photon: $\mathcal{A} = \bar{\epsilon}_{\rm IC}(\gamma)/\gamma$. This quantity is shown in Fig. 4 for the case of a mono-energetic ambient photon field.

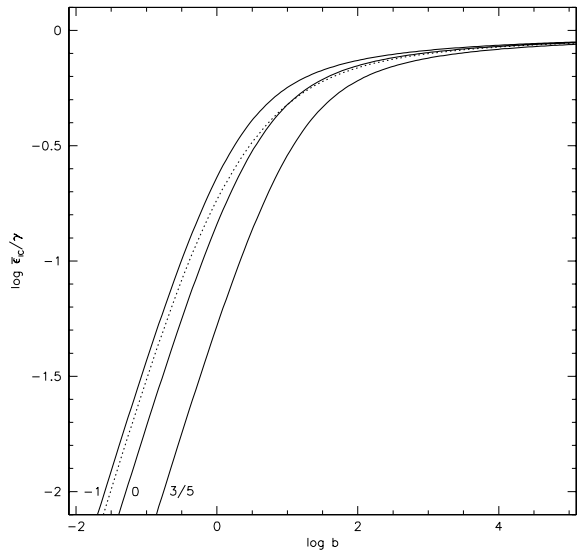

Figure 4. Inelasticity, $\mathcal{A} = \bar{\epsilon}_{\rm IC}(\gamma)/\gamma$ for electron Compton scatterings off a mono-energetic ambient radiation field: dotted line, isotropic ambient radiation field; solid lines, beamed ambient radiation field, for scattering angles $\cos\theta = -1.0$, 0.0 and 0.6.

Inserting the delta function approximation into equations (15) and (16), we can rewrite the IC emissivities as

$$\epsilon j_{\epsilon(\mathrm{IC})}(\theta) \simeq \frac{n_\gamma \gamma}{4\pi} |\dot{\gamma}|_{\mathrm{IC}} m_\mathrm{e} c^2 \chi(\gamma, \theta) \frac{\mathrm{d} \ln \gamma}{\mathrm{d} \ln \bar{\epsilon}_{(\mathrm{IC})}(\theta)}, \tag{19}$$

and

$$\epsilon j_{\epsilon(\mathrm{IC})} \simeq \frac{n_\gamma \gamma}{4\pi} |\dot{\gamma}|_{\mathrm{IC}} m_\mathrm{e} c^2 \frac{\mathrm{d} \ln \gamma}{\mathrm{d} \ln \bar{\epsilon}_{(\mathrm{IC})}}, \tag{20}$$

respectively, where

$$\chi(\gamma, \theta) = \frac{\int f(\epsilon, \epsilon_0, \gamma, \theta) \epsilon \, \mathrm{d}\epsilon}{\int f_{\mathrm{iso}}(\epsilon, \epsilon_0, \gamma) \epsilon \, \mathrm{d}\epsilon} \equiv \frac{\bar{\epsilon}_{\mathrm{IC}}(\gamma, \theta)}{\bar{\epsilon}_{\mathrm{IC}}(\gamma)}. \tag{21}$$

Note that in the Thomson limit, $\bar{\epsilon}_{\mathrm{IC}} \propto \gamma^2$, so that $\mathrm{d} \ln \gamma / \mathrm{d} \ln \bar{\epsilon}_{\mathrm{IC}} = 1/2$, while in the KN limit, $\bar{\epsilon}_{\mathrm{IC}} \sim \gamma$, so that $\mathrm{d} \ln \gamma / \mathrm{d} \ln \bar{\epsilon}_{(IC)} = 1$.

We can make an analogous approximation for the synchrotron emissivity, provided that the magnetic fields are isotropic and $\gamma_{\max} < B_{\mathrm{cr}}/(4B)$. We have then,

$$\epsilon j_{\epsilon(\mathrm{syn})} \simeq \frac{n_\gamma \gamma}{4\pi} |\dot{\gamma}|_{\mathrm{syn}} m_\mathrm{e} c^2 \frac{\mathrm{d} \ln \gamma}{\mathrm{d} \ln \bar{\epsilon}_{(\mathrm{syn})}} = \frac{1}{2} \frac{n_\gamma \gamma}{4\pi} |\dot{\gamma}|_{\mathrm{syn}} m_\mathrm{e} c^2 \tag{22}$$

where $\bar{\epsilon}_{\mathrm{syn}} = (4/3)\gamma^2 (B/B_{\mathrm{cr}})$ and $B_{\mathrm{cr}} \equiv 2\pi m_\mathrm{e}^2 c^3/(he) \simeq 4.4 \times 10^{13}$ G.

4 STEADY-STATE ELECTRON ENERGY DISTRIBUTION

Under the assumptions that the time-scales for the acceleration of individual electrons are much shorter than the time-scales of their energy losses, that electrons do not escape from the cooling region, and that they also do not suffer adiabatic losses, the evolution of the electron energy distribution, n_γ, can be described by the integro-differential equation (Blumenthal & Gould 1970)

$$\frac{\partial n_\gamma}{\partial t} = -\frac{\partial}{\partial \gamma}(n_\gamma |\dot{\gamma}|) - n_\gamma \int_1^\gamma C(\gamma, \gamma') \, \mathrm{d}\gamma' + \int_\gamma^{\gamma_{\max}} n_\gamma C(\gamma', \gamma) \, \mathrm{d}\gamma' + Q, \tag{23}$$

where $|\dot{\gamma}|$ is the energy loss rate due to loss processes that may be approximated as being continuous, e.g. synchrotron radiation, $C(\gamma, \gamma')$ is the probability per unit time for Compton scattering of an electron with energy γ to energy γ', and Q is the electron injection function, i.e. the electron production rate per unit time, per energy and per volume. The transition rates $C(\gamma, \gamma')$ have been derived by Jones (1968) for a mono-energetic ambient radiation field, and by Zdziarski (1988) for power-law ambient radiation fields.

To illustrate in a simple way the effects of KN corrections, we use a continuity version of the kinetic equation

$$\frac{\partial n_\gamma}{\partial t} = -\frac{\partial}{\partial \gamma}(n_\gamma |\dot{\gamma}|_{\mathrm{tot}}) + Q, \tag{24}$$

despite the fact that in the KN regime the fractional electron energy losses per scattering are not negligible (see Fig. 4). Such a simplification can be justified by noting that the results obtained by Zdziarski (1989) show that the electron distributions obtained by using the exact integro-differential equation versus the continuity equation are qualitatively very similar and that significant differences (up to a factor few) occur only if both the electron injection function and the ambient radiation field are mono-energetic. In the cases studied here, the differences are further reduced by the increasingly important role of the (continuous) synchrotron energy losses at the highest energies, particularly if $b_{\max} > b_\mathrm{s}$. We demonstrate this explicitly in Figs 5–7 where we compare the results of exact

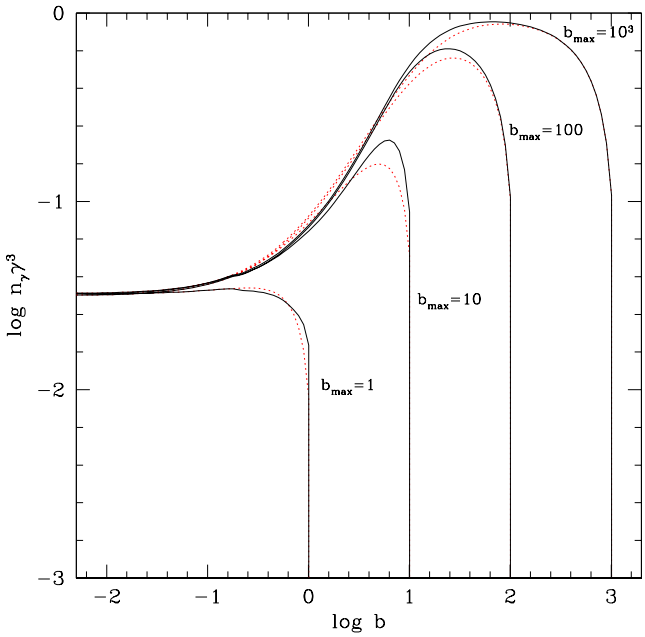

Figure 5. Steady-state electron energy distributions for the power-law electron injection function, $Q \propto \gamma^{-p}$, and mono-energetic ambient radiation field: solid lines, exact results; dotted lines, results obtained using the continuous energy loss approximation for all Compton scattering. The model parameters are: $p = 2$, $q = 30$; $b_{\max} = 1$; 10; 100; 10^3.

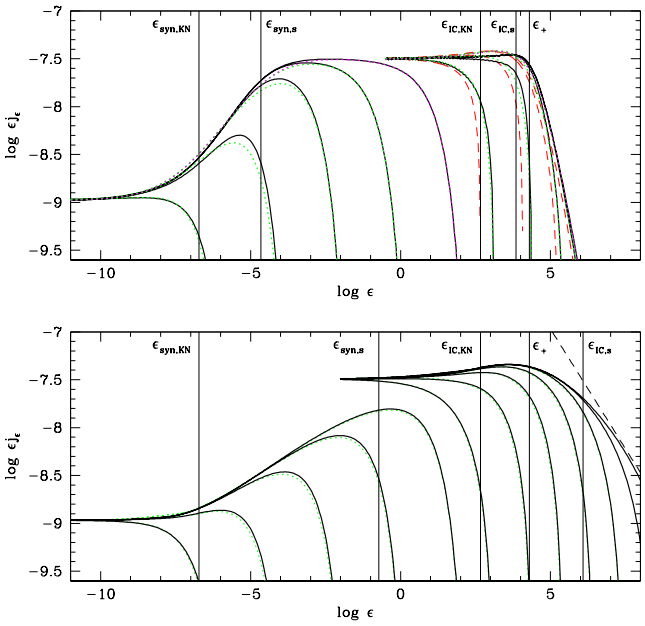

Figure 6. IC plus synchrotron spectra of steady sources with model parameters $p = 2$; $q = 30$; $b_{\max} = 1$, 10, 10^2, 10^3, 10^4; $\epsilon_0 = 10^{-4}$; $B = 1$ G. Upper panel: mono-energetic ambient radiation field. Lower panel: power-law ambient radiation field with $\alpha_0 = 0.5$. Solid lines denote exact calculations. Dotted lines denote calculations using continuous energy loss approximation. Dashed lines denote Compton spectra computed using the continuous energy loss approximation and the delta function approximation. The dot-dashed line in the lower panel is the asymptotic power law ($\alpha = -0.5$) for the IC spectrum at $\epsilon > \epsilon_{\mathrm{IC,s}}$ given by equation (27). To show convergence to this spectrum for increasing $b_{\max}$, the lower panel also shows the IC spectra obtained for $b_{\max} = 10^5$, 10^6 and 10^7.

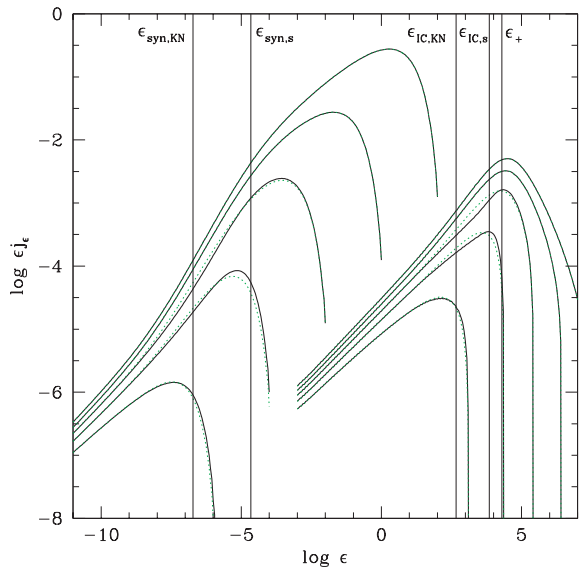

Figure 7. Same as the upper panel of Fig. 6 (mono-energetic radiation field), but for $p = 1$.

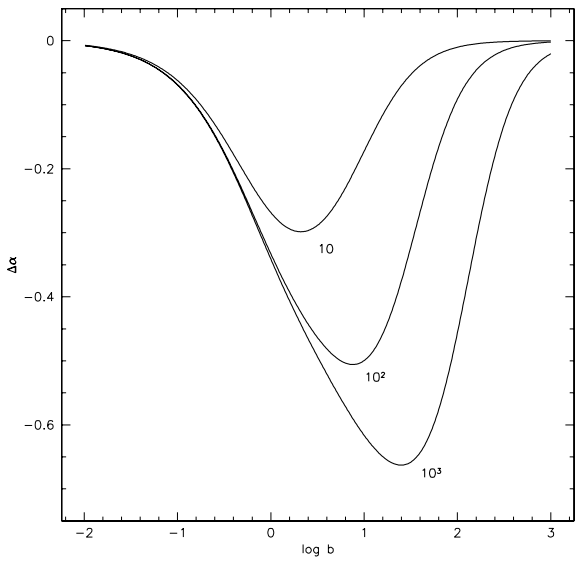

Figure 8. Synchrotron spectral 'hardening', $\Delta\alpha$, as a function of b. Model parameters: $b_{\rm max} = \infty$, and $q = 10, 10^2, 10^3$.

calculations made using the code of Coppi (1992) with the approximate results obtained by treating Compton losses continuously in that code. For many applications that do not involve fitting data and thus do not require very high accuracy, the continuous energy loss approximation should suffice.

A steady-state solution of the continuity equation, $\partial n_\gamma/\partial t = 0$, is

$$n_\gamma = \frac{1}{|\dot\gamma_{\rm tot}|}\int_\gamma Q\,{\rm d}\gamma = \frac{3m_{\rm e}c}{4\sigma_{\rm T}u_B}\frac{\int_\gamma Q\,{\rm d}\gamma}{\gamma^2(1+qF_{\rm KN})}, \tag{25}$$

where we assume that electron energy losses are dominated by the IC process and by synchrotron radiation, i.e. that

$$|\dot\gamma_{\rm tot}| = |\dot\gamma_{\rm syn}| + |\dot\gamma_{\rm IC}| = \frac{4c\sigma_{\rm T}u_B}{3m_{\rm e}c^2}\gamma^2(1+qF_{\rm KN}). \tag{26}$$

For $b_{\rm max} \gg b_{\rm s}$ and $q \gg 1$, the steady-state distribution has two asymptotes: one for $b \ll 1$, where electron energy losses are dominated by Thomson scatterings, i.e. $F_{\rm KN} = 1$; and one for $b_{\rm s} \ll b \ll b_{\rm max}$, where electron energy losses are dominated by synchrotron radiation, i.e. $qF_{\rm KN} \ll 1$. The respective equilibrium electron distributions are $\gamma^2 n_\gamma \propto \int_\gamma Q\,{\rm d}\gamma/(1+q)$ and $\gamma^2 n_\gamma \propto \int_\gamma Q\,{\rm d}\gamma$. For $1 < b < b_{\rm s}$, despite the decrease of the KN cross-section, electron energy losses are still dominated by the IC process and the electron distribution is $\gamma^2 n_\gamma \propto \int_\gamma Q\,{\rm d}\gamma/(qF_{\rm KN})$.

For a rapid acceleration mechanism that produces a power-law electron injection spectrum, $Q \propto \gamma^{-p}$, with $p > 1$, the two asymptotes of the steady-state distribution (for $b \ll 1$ and $b \gg b_{\rm s}$) are power laws with the same spectral index, $s = p + 1$, where $s \equiv -{\rm d}\ln n_\gamma/{\rm d}\ln\gamma$. For $1 \ll b \ll b_{\rm s}$, i.e. for $\gamma_{\rm KN} < \gamma < \gamma_{\rm s}$, the electron distribution is harder than in the asymptotic regions, with a spectral index reaching $s = p + 1 + \Delta s$, where $\Delta s \simeq {\rm d}\ln F_{\rm KN}/{\rm d}\ln\gamma < 0$. Using the analytical approximations for $F_{\rm KN}$ given in Section 2 and going to the limit $q \gg 1$, we find that for ambient radiation fields with mono-energetic or very sharply peaked photon energy distributions, $\Delta s \simeq -1.5$, while for softer external fields, with $\alpha_0 > 0.0$, $\Delta s \simeq \alpha_0 - 1$. When $q \lesssim 10^3$, the maximum hardening, Δs, of the electron distribution is a function of q and decreases with decreasing q. (See Fig. 8 for an example of how the corresponding hardening of the electron synchrotron depends on q.) Note that this result is independent of the injection index p as long as the continuous Compton cooling approximation holds. Of course, for $b_{\rm max} < b_{\rm s}$ the electron energy distribution will not have the maximum deviation possible from the Thomson-limit ($b \ll 1$) asymptote and Δs may not reach its maximum value. In this case, the KN induced bump or 'excess' at the high-energy end of the electron distribution is correspondingly less prominent. This is demonstrated in Fig. 5, where the electron distribution is computed for four different values of $b_{\rm max}$.

5 SPECTRA

5.1 Klein–Nishina effects

Examples of the steady-state electromagnetic spectra produced for the case of power-law electron injection function are shown in Figs 6 and 7. The IC spectra are computed assuming an isotropic ambient radiation field. The characteristic photon energies marked on the figures have the following definitions (see equation 18): $\epsilon_{\rm IC,KN} \equiv \bar\epsilon_{\rm IC}(\gamma_{\rm KN})$; $\epsilon_{\rm IC,s} \equiv \bar\epsilon_{\rm IC}(\gamma_{\rm s})$; $\epsilon_{\rm syn,KN} \equiv \bar\epsilon_{\rm syn}(\gamma_{\rm KN})$; $\epsilon_{\rm syn,s} \equiv \bar\epsilon_{\rm syn}(\gamma_{\rm s})$; and $\epsilon_+ \equiv 2/\epsilon_{0,\rm max}$, which is the approximate threshold energy for photon–photon pair production on the ambient photon distribution.

As one can see, the high-energy parts of the IC and synchrotron spectra behave very differently. The IC spectra do not change very much after crossing $\epsilon_{\rm IC,KN}$. This is because for $q \gg 1$, Compton scattering still dominates the cooling of the electrons responsible for IC photons at $\epsilon \gtrsim \epsilon_{\rm IC,KN}$. Even though those electrons scatter in the KN regime, the decreased efficiency of Compton scattering is compensated by the corresponding increase in their equilibrium density, as discussed in Zdziarski & Krolik (1993). As one moves to higher photon energies, however, synchrotron cooling becomes relatively more important for the electrons responsible for these IC photons. Eventually, when the energy of the relevant electrons exceeds $\gamma_{\rm s}$, synchrotron cooling rapidly dominates and the fraction of the electron's energy going into the Compton component plummets. The result is a sharp steepening or break of the IC spectrum at energy $\epsilon_{\rm IC,s}$, which is independent of the maximum electron energy $\gamma_{\rm max} > \gamma_{\rm s}$.

When one instead considers synchrotron emission, the hardening of the electron distribution at $\gamma > \gamma_{\rm KN}$ is directly reflected in the synchrotron spectrum. The result is a synchrotron spectrum that can harden dramatically at $\epsilon > \epsilon_{\rm syn,KN}$, forming a synchrotron 'bump' if $b_{\rm max} < b_{\rm s}$. Note that if $q \gg 1$, the hardening of the synchrotron component can already be noticeable at even lower energies, $\sim\bar{\epsilon}_{\rm syn}(0.1\gamma_{\rm KN})$. For $b_{\rm max} \gg b_{\rm s}$, the synchrotron spectrum at $\epsilon > \epsilon_{\rm syn,s}$ converges to a spectrum with the same slope as the low-energy (Thomson regime) asymptote but with a normalization that is a factor q higher.

An interesting consequence of the very different behaviours of the high-energy portions of IC and synchrotron spectra is that for the case of a flat electron injection spectrum ($p < 2$) with $b_{\rm max} > b_{\rm s}$, the luminosity of the synchrotron peak – located around $\epsilon_{\rm syn,max} \equiv \bar{\epsilon}_{\rm syn}(\gamma_{\rm max})$ – will exceed the luminosity of the IC peak (located around $\epsilon_{\rm IC,s}$), no matter how large we make q. This dominance of the synchrotron component, even though $q = 30 \gg 1$, is demonstrated in Fig. 7.

All the spectral features just described can be reproduced analytically, by using the equations

$$\epsilon\, j_{\epsilon({\rm IC})} \simeq \frac{m_{\rm e}c^2}{4\pi}\frac{q F_{\rm KN}}{1+q F_{\rm KN}}\gamma\int_{\gamma} Q\,{\rm d}\gamma\,\frac{{\rm d}\ln\gamma}{{\rm d}\ln\bar{\epsilon}_{\rm IC}} \tag{27}$$

and

$$\epsilon\, j_{\epsilon({\rm syn})} \simeq \frac{1}{2}\frac{m_{\rm e}c^2}{4\pi}\frac{1}{1+q F_{\rm KN}}\gamma\int_{\gamma} Q\,{\rm d}\gamma, \tag{28}$$

which are obtained after insertion of equation (25) into equations (20) and (22), respectively. For $\gamma_{\rm max} \gg \gamma_{\rm s}$ and $q \gg 1$, the latter implying $b_{\rm s} \gg 1$, i.e. $\gamma_{\rm s} \gg \gamma_{\rm KN}$, the IC and synchrotron spectra can be characterized as the superposition of three components produced by electrons with $\gamma \ll \gamma_{\rm KN}$, $\gamma_{\rm KN} \ll \gamma \ll \gamma_{\rm s}$ and $\gamma_{\rm s} \ll \gamma \ll \gamma_{\rm max}$. These components are

$$\frac{4\pi\epsilon\, j_{\epsilon({\rm IC})}}{m_{\rm e}c^2} \sim \gamma\int_{\gamma} Q\,{\rm d}\gamma \begin{cases} 1/2 & \text{if } \epsilon \ll \epsilon_{\rm IC,KN} \\ 1 & \text{if } \epsilon_{\rm IC,KN} \ll \epsilon \ll \epsilon_{\rm IC,s} \\ q F_{\rm KN} & \text{if } \epsilon_{\rm IC,s} \ll \epsilon \ll \epsilon_{\rm IC,max} \end{cases}, \tag{29}$$

where $\gamma \simeq \sqrt{(3/4)(\epsilon/\epsilon_{0,\rm max})}$ if $\epsilon \ll \epsilon_{\rm IC,KN}$, and $\epsilon \simeq \gamma$ if $\epsilon \gg \epsilon_{\rm IC,KN}$, and

$$\frac{4\pi\epsilon\, j_{\epsilon({\rm syn})}}{m_{\rm e}c^2} \sim \gamma\int_{\gamma} Q\,{\rm d}\gamma \times \begin{cases} 1/(2q) & \text{if } \epsilon \ll \epsilon_{\rm syn,KN} \\ 1/(2q F_{\rm KN}) & \text{if } \epsilon_{\rm syn,KN} \ll \epsilon \ll \epsilon_{\rm syn,s} \\ 1/2 & \text{if } \epsilon_{\rm syn,s} \ll \epsilon \ll \epsilon_{\rm syn,max} \end{cases}, \tag{30}$$

where $\gamma = \sqrt{3\epsilon B_{\rm cr}/(4B)}$.

For electron injection $Q \propto \gamma^{-p}$ and $p > 1$, the various components are power laws, i.e. we have

$$\frac{4\pi\epsilon\, j_{\epsilon({\rm IC})}}{m_{\rm e}c^2} \propto \begin{cases} \epsilon^{-p/2} & \text{if } \epsilon \ll \epsilon_{\rm IC,KN} \\ \epsilon^{-(p-1)} & \text{if } \epsilon_{\rm IC,KN} \ll \epsilon \ll \epsilon_{\rm IC,s} \\ \epsilon^{-(p-1+\delta\alpha)} & \text{if } \epsilon_{\rm IC,s} \ll \epsilon \ll \epsilon_{\rm IC,max} \end{cases}, \tag{31}$$

where $\delta\alpha \sim 1.5$ for $\alpha_0 < -1$, and $\delta\,\alpha \sim 1 - \alpha_0$ for $0 < \alpha_0 < 1$, while

$$\frac{4\pi\epsilon\, j_{\epsilon({\rm syn})}}{m_{\rm e}c^2} \propto \begin{cases} \epsilon^{-p/2} & \text{if } \epsilon \ll \epsilon_{\rm syn,KN} \\ \epsilon^{-(p/2+\Delta\alpha)} & \text{if } \epsilon_{\rm syn,KN} \ll \epsilon \ll \epsilon_{\rm syn,s} \\ \epsilon^{-p/2} & \text{if } \epsilon_{\rm syn,s} \ll \epsilon \ll \epsilon_{\rm syn,max} \end{cases}, \tag{32}$$

where $\Delta\alpha = -[{\rm d}\ln(1/F_{\rm KN})/{\rm d}\ln\varepsilon]|_{b\propto\varepsilon^{1/2}}$. For $\alpha_0 < -1$, $\Delta\alpha \sim -0.75$, while for $0 < \alpha_0 < 1$, $\Delta\alpha \sim -(1-\alpha_0)/2$. We should emphasize here that estimation of the hardening of synchrotron spectrum slope in the band $[\epsilon_{\rm syn,KN};\, \epsilon_{\rm syn,s}\,]$ is very crude and corresponds to its maximum value, which as noted previously, can be reached only for $q \gtrsim 10^3$. As shown in Fig. 8, the synchrotron spectral hardening will be weaker for lower values of q.

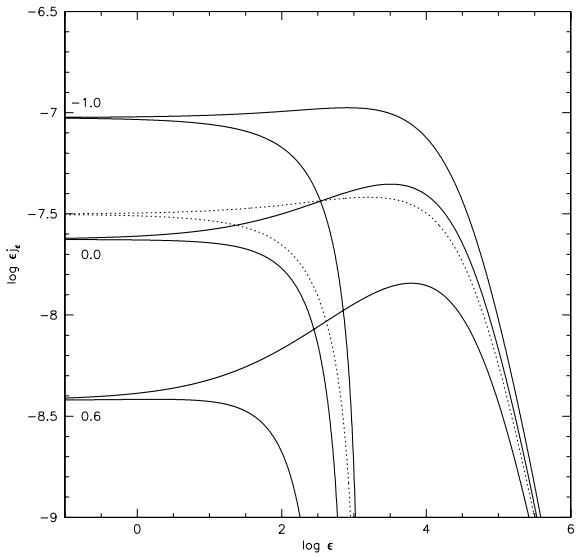

Figure 9. IC spectra for a beamed ambient radiation field. The model parameters are: $q = 30$, $b_{\rm max} = 10,\, 10^3$; $\epsilon_0 = 10^{-4}$; $\cos\theta = -1.0,\, 0.0,\, 0.6$. For comparison, the IC spectra for an isotropic ambient radiation field are also shown (dotted lines).

Although we have only presented and discussed emission spectra computed for an isotropic ambient radiation field, we would like to emphasize that with our generic assumption of isotropic distribution of electrons, the electron energy losses, as well as the distribution of electrons (equation 25) and their synchrotron emissivity (equation 22), do not depend on the angular distribution of the ambient radiation field. Hence, in the case of a beamed ambient radiation field, the IC spectrum can be simply computed from equations (15) or (19) by using the electron distribution given by equation (25). In Fig. 9 we show such spectra for three different scattering angles and compare them with that computed for the isotropic ambient radiation field. One can see that the deeper one is in the KN regime, the weaker is anisotropy of the scattered radiation. Suppression of the anisotropy is caused by the recoil effect.

5.2 Further effects that may modify the observed spectrum

To highlight the spectral effects caused by the modification of the electron energy distribution due to Compton scatterings in the KN regime, we have considered only spectra produced in the fast electron cooling regime, and we have ignored possibly important processes such as photon–photon pair production and synchrotron self-Compton radiation. We also did not consider effects due to the relativistic propagation of the source, which is important in objects such as blazars. We discuss below how our results can be affected by the inclusion of some of these complications.

5.2.1 Fast versus slow cooling regime

Assuming that electron energy losses are dominated by radiative processes, the cooling time-scale for an electron of energy γ is (see

equation 26)

$$t_{\rm c} \equiv \frac{\gamma}{|\dot{\gamma}|} = \frac{3m_{\rm e}c}{4\sigma_{\rm T}u_B\gamma(1+qF_{\rm KN})}. \quad (33)$$

For sources with a finite (comoving frame) lifetime t_Q, the only electrons that have time to cool significantly are those with $t_{\rm c} < t_Q$. Looking first at the Thomson limit ($\gamma \lesssim \gamma_{\rm KN}$) of this expression, we find the usual result that only electrons with $\gamma > \gamma_{\rm c}$ have time to cool, where

$$\gamma_{\rm c} = \frac{3m_{\rm e}c}{4\sigma_{\rm T}u_0 t_Q} \quad (34)$$

for $q \gg 1$. The number density of electrons at a given energy that can accumulate in the source is roughly $Q(\gamma)\min[t_{\rm c}(\gamma), t_Q]$. For power-law electron injection, the electron energy distribution of electrons therefore hardens by $\Delta s = 1$ for $\gamma < \gamma_{\rm c}$, leading to a hardening of the synchrotron or Compton spectrum by $\Delta\alpha = 0.5$.

For $\gamma > \gamma_{\rm KN}$, $q \gg 1$, and a mono-energetic ambient photon distribution, the cooling time increases for $\gamma > \gamma_{\rm KN}$, reaching a local maximum at $\gamma \approx \gamma_{\rm s}$, when synchrotron cooling begins to dominate. Efficient KN cooling therefore requires $t_{\rm c}(\gamma_{\rm s}) < t_Q$. From equation (33), we have

$$t_{\rm c}(\gamma_{\rm s}) = \frac{3m_{\rm e}c}{8\sigma_{\rm T}u_B\gamma_{\rm s}} = \frac{3m_{\rm e}c\epsilon_0}{2\sigma_{\rm T}u_0}\frac{q}{b_{\rm s}}. \quad (35)$$

Hence, fast cooling in the KN regime requires

$$\frac{q}{b_{\rm s}} < \frac{2\sigma_{\rm T}u_0 t_Q}{3\epsilon_0 m_{\rm e}c} \quad (36)$$

or, equivalently using $b_{\rm s} \sim q^{2/3}$ for $1 \ll q \lesssim 10^3$,

$$q < \left(\frac{2\sigma_{\rm T}u_0 t_Q}{3\epsilon_0 m_{\rm e}c}\right)^3. \quad (37)$$

Of course, if we have $b_{\rm max} < b_{\rm s}$, the upper limit on q is correspondingly weaker.

For a power-law photon distribution with $0 \lesssim \alpha_0 \lesssim 1$, we may use equation (33) and approximation (6) to show that $t_{\rm c} \sim \gamma^{-\alpha_0}$. For $\alpha_0 > 0$, this is a monotonically decreasing function of γ, so fast cooling throughout the KN regime is simply guaranteed by the condition $t_{\rm c}(\gamma_{\rm KN}) \leqslant t_Q$, or equivalently $\gamma_{\rm KN} > \gamma_{\rm c}$. This can be translated into the following requirement on the energy density of the external radiation field,

$$u_0 > \frac{3m_{\rm e}c}{4\gamma_{\rm KN}\sigma_{\rm T}t_Q} = \frac{3m_{\rm e}c\epsilon_0}{\sigma_{\rm T}t_Q}. \quad (38)$$

For a photon distribution that is harder than $\alpha_0 = 0$ or softer than $\alpha_0 = 1$, i.e. for a radiation field that is effectively mono-energetic (see discussion in Section 2.1), we must instead require $t_{\rm c}(\gamma_{\rm s}) \leqslant t_Q$.

5.2.2 *Photon–photon pair production*

Because (i) the cross-section for photon–photon pair production is similar in magnitude to that for Compton scattering, and (ii) the photon threshold energy for pair production, $\epsilon_+ \sim 1/\epsilon_{0,\rm max}$, is almost the same as the electron energy $\gamma_{\rm KN} \sim 1/\epsilon_{0,\rm max}$, it is often stated that strong pair production is unavoidable in sources where KN effects are important. This is not always true, however.

First, in many applications a better estimate for the threshold energy is in fact $\epsilon_+ = 2/\epsilon_{0,\rm max}$. Moreover, KN effects are actually important at energies well below $1/\epsilon_{0,\rm max}$, i.e. at $\gamma < \gamma_{\rm KN} = 1/4\epsilon_{0,\rm max}$. Furthermore, from Fig. 4, $\mathcal{A}(\gamma_{\rm KN}) \sim 0.1$–$0.3$, so that an electron of energy $\gamma_{\rm KN}$ actually Compton up-scatters photons to typical energies $\epsilon_{\rm IC,KN} = \mathcal{A}_{\rm KN}\gamma_{\rm KN} \ll \epsilon_+$. Taking $\mathcal{A}$ at larger energies to be $\sim$0.5, we see that we in fact need a source with $b_{\rm max} > b_+ = \gamma_+/\gamma_{\rm KN} \sim \simeq 16$. Because KN distortions of the electron spectrum already produce visible distortions in the synchrotron spectrum for electron energies $b \sim 0.1$, this means there is a factor of $\sim$100 in electron energy for which KN corrections are important but pair production is not possible. Because $\bar{\epsilon}_{\rm syn} \propto b^2$, this corresponds to a factor of 10^4 in synchrotron frequency.

Secondly, even if we have $b_{\rm max} \gtrsim b_+$, pair production may still not be important. When one includes the effects of synchrotron cooling, left out of KN pair production studies such as Zdziarski (1988), we have seen that one obtains a strong break at $\epsilon_{\rm IC,s}$ corresponding to the electron energy $b_{\rm s}$ where synchrotron cooling starts to dominate. Thus, if $b_+ < b_{\rm max}$ but $b_+ > b_{\rm s}$, pair production occurs but the luminosity of the pairs that are produced (and the spectral distortions they induce) will not be bolometrically important. For a mono-energetic photon distribution, $b_{\rm s} \simeq q^{2/3}$, and one thus has $b_{\rm s} < b_+$ for any $q \lesssim 60$, independent of the actual value of the maximum electron energy, $b_{\rm max}$, e.g. see Figs 6(a) and 7. Note, though, that for an ambient photon distribution that is not mono-energetic, e.g. a power law with $\alpha_0 \gtrsim -0.5$, KN effects are not as strong as for the mono-energetic case because lower-energy photons that scatter in the Thomson regime are available. The spectral break due to $\epsilon_{\rm IC,s}$ therefore occurs at higher energy and pair production can be important for much lower q, e.g. see Fig. 6(b).

Even if pair production is energetically possible, the preceding discussion says nothing about whether the optical depth to pair production $\tau_{\gamma\gamma}$ actually exceeds unity, and it ignores the effects of photon anisotropy (which raise the pair production threshold). In a realistic source, the extent and geometry of the external radiation field must be taken into account as well as its absolute intensity. In galactic pulsar wind applications, for example, the ambient radiation field due to the companion star is often highly anisotropic in the source region of interest. In the most general case, $\tau_{\gamma\gamma}$ must be treated as a free parameter. In particular, if the source region has an effectively infinite lifetime and is not expanding, which avoids the problem of adiabatic losses, we are essentially free to choose as low an external field energy density as we like without violating the fast KN cooling constraints discussed above. If the source is not static, though, there are interesting limits we can place on $\tau_{\gamma\gamma}$ if we demand efficient KN cooling. For example, consider a source of size R with a characteristic lifetime or expansion time-scale $\sim R/c$. For simplicity, assume also that the radiation field is mono-energetic. Then, taking $\tau_{\gamma\gamma} \simeq 0.2 n_0\sigma_{\rm T}R$ where $n_0 = u_0/\epsilon_0$ and using the fast-cooling condition of equation (35), we have

$$\tau_{\gamma\gamma} \gtrsim \frac{3}{10}q^{1/3}. \quad (39)$$

This implies, for example, that we can be in the fast KN regime and still have $\tau_{\gamma\gamma} < 1$ for $q \lesssim 37$.

5.2.3 *Up-scattering of photons produced inside the source*

The steady-state distribution of electrons comes from balancing the injection of electrons by their radiative energy losses and, in general, one should include both up-scattering of photons produced outside the source as well as up-scattering of photons produced inside the source. The latter involves the synchrotron-self Compton (SSC) process and multiple-Compton scatterings of photons resulting from Comptonization of external radiation and from Comptonization of SSC photons. These processes (SSC + multiple-Compton

scatterings) are assumed in the present work to have negligible effects on the electron energy distribution. The assumption can be justified by comparison of a rate of energy losses via SSC and multiple-Compton scatterings, $\dot{\gamma}_{\rm SSC+MC}$, with the total energy losses rate, $\dot{\gamma}_{\rm tot}$. We have

$$\dot{\gamma}_{\rm SSC+MC} \propto \int f_{\rm KN} u_\epsilon \, {\rm d}\epsilon \tag{40}$$

and

$$\dot{\gamma}_{\rm tot} \propto u_B + \int f_{\rm KN} u_{\epsilon_0} \, {\rm d}\epsilon_0 + \int f_{\rm KN} u_\epsilon \, {\rm d}\epsilon, \tag{41}$$

where u_ϵ is the energy density of the radiation emitted within the source (it includes all radiative components: synchrotron, SSC, Comptonized external radiation, SSC and higher-order Compton components). In the steady-state case

$$\int u_\epsilon {\rm d}\epsilon = u_{\rm inj} \equiv \frac{R}{c} \int Q(\gamma - 1) m_{\rm e} c^2 \, {\rm d}\gamma, \tag{42}$$

and introducing the new parameter, $q_{\rm inj} \equiv u_{\rm inj}/u_B$, we obtain

$$\frac{\dot{\gamma}_{\rm SSC+MC}}{\dot{\gamma}_{\rm tot}} = \frac{q_{\rm inj} F_{\rm KN(inj)}}{1 + q F_{\rm KN} + q_{\rm inj} F_{\rm KN(inj)}}, \tag{43}$$

where $F_{\rm KN(inj)} = (1/u_{\rm inj}) \int f_{\rm KN} u_\epsilon \, {\rm d}\epsilon$. Hence, $\dot{\gamma}_{\rm SSC+MC}/\dot{\gamma}_{\rm tot} \ll 1$ if $q_{\rm inj} \ll q$, i.e. if $u_{\rm inj} \ll u_{\rm ext}$. In particular, if energy injected via electrons is equiparteted with magnetic fields, i.e. $q_{\rm inj} \sim 1$, then the effects of SSC and of multiple-Compton scatterings on the electron energy distribution are negligible for any $q \gg 1$.

5.2.4 Relativistic source propagation effects

If a source is moving with relativistic speed (bulk Lorentz factor $\Gamma \gg 1$), and the external radiation field in such a frame is isotropic, and with an energy density u_0 peaked at photon energies $\sim\epsilon_0$, then in the source rest frame, the energy density of the external radiation is Γ^2 times larger and the energies of seed photons are Γ times higher. Then the rest-frame quantities relevant to our discussion of KN effects are $b = 4\,\Gamma\gamma\epsilon_0$, and, in particular, $\gamma_{\rm KN} \simeq 1/(4\,\Gamma\gamma\epsilon_0)$, and $q \simeq \Gamma^2 u_0/u_B$. Because for $\Gamma \gg 1$ the head-on approximation applies, the IC emissivity can be computed using equation (15) with

$$\cos\theta = -\cos\psi'_{\rm obs} = -\frac{\cos\psi_{\rm obs} - \beta}{1 - \beta\cos\psi_{\rm obs}}, \tag{44}$$

where $\psi'_{\rm obs}$ is the angle between the jet axis and the direction to the observer in the comoving frame while $\psi_{\rm obs}$ is the same angle but as measured in the lab frame. The observed source flux is then

$$\epsilon_{\rm obs} F_{\epsilon_{\rm obs}} = \frac{\mathcal{D}^4 \int \epsilon \, j_\epsilon(\theta) \, {\rm d}V}{d_L^2}, \tag{45}$$

where $\epsilon_{\rm obs} = \epsilon\mathcal{D}/(1+z)$, $\mathcal{D} = 1/[\Gamma(1-\beta\cos\psi_{\rm obs})]$ is the Doppler factor, d_L is the distance (luminosity distance for cosmological objects), z is the redshift, and V is the volume of the source as measured in its rest frame. The lifetime of the source measured in the lab frame is Γt_Q.

6 APPLICATIONS

6.1 Blazars

The clearest and probably the most numerous examples of high-q (radiation-dominated) non-thermal sources are FSRQs – radio-loud quasars seen at small angles to the jet axis. Many of these are categorized as optically violent variables (OVVs) and/or highly polarized quasars (HPQs), and together with on average much less luminous BL Lac objects, they form the subclass of AGNs called 'blazars'. The Doppler boosted non-thermal radiation from quasar jets is often strongly dominated by gamma-rays (von Montigny et al. 1995; Mukherjee et al. 1997). Day–week variability time-scales suggest that these sources are located at (sub)parsec distances from the centre. There, the external radiation field, as viewed in the jet comoving frame, is dominated by the powerful broad emission line (BEL) region radiation. For $u_0 \simeq L_{\rm BEL}/(4\pi r_{\rm BEL}^2 c)$ and $u_B \simeq L_B/[\pi(r\theta_j)^2 c\Gamma^2]$

$$q(r \sim r_{\rm BEL}) \simeq \frac{\Gamma^2 u_0}{u_B} \simeq 25 \frac{L_{\rm BEL,45}(\Gamma/10)^2(\Gamma\theta_j)^2}{4L_{B,45}}, \tag{46}$$

where L_B is the magnetic energy flux carried by the jet and $\theta_j = R/r$ is the half-opening angle of a jet.

Let us determine now the values of $\gamma_{\rm KN}$ and $\gamma_{\rm s}$ and the corresponding IC and synchrotron photon energies for such an external radiation field, assuming that $q \gg 1$ and $\gamma_{\rm max} > \gamma_{\rm s}$. Noting that the energies of BELs peak around $\sim$10 eV ($\epsilon_0 \approx 2 \times 10^{-5}$) and that they are seen in the jet comoving frame as boosted by a factor $\sim\Gamma$, i.e. $b = 4\epsilon_0\gamma\Gamma$, we have

$$\gamma_{\rm KN} = \frac{1}{4\epsilon_0\Gamma} \sim 10^3(\Gamma/10)^{-1} \tag{47}$$

and

$$\gamma_{\rm s} = b_{\rm s}\gamma_{\rm KN} \sim 10^4(q/30)^{2/3}(\Gamma/10)^{-1}. \tag{48}$$

These electrons Comptonize external photons up to average energies

$$\epsilon^{\rm obs}_{\rm IC,KN} \simeq \mathcal{A}_{\rm KN}\gamma_{\rm KN}\mathcal{D} \sim 2 \times 10^3(\mathcal{A}_{\rm KN}/0.14)(\mathcal{D}/\Gamma) \quad (\sim 1\,{\rm GeV}\ldots) \tag{49}$$

and

$$\epsilon^{\rm obs}_{\rm IC,s} \simeq \mathcal{A}_s\gamma_{\rm s}\mathcal{D} \simeq 6 \times 10^4(\mathcal{A}_s/0.5)(q/30)^{2/3}(\mathcal{D}/\Gamma) \quad (\sim 30\,{\rm GeV}\ldots), \tag{50}$$

and produce synchrotron photons with average energies

$$\epsilon^{\rm obs}_{\rm syn,KN} = \frac{4}{3}\gamma^2_{\rm KN}\frac{B}{B_{\rm cr}}\mathcal{D} \sim 2 \times 10^{-7}\frac{L^{1/2}_{B,45}(\mathcal{D}/\Gamma)}{R_{\rm BEL,18}(\Gamma/10)} \quad (\sim 3 \times 10^{13}\,{\rm Hz}\ldots), \tag{51}$$

$$\epsilon^{\rm obs}_{\rm syn,s} = b^2_{\rm s}\epsilon^{\rm obs}_{\rm syn,KN} \simeq q^{4/3}\epsilon^{\rm obs}_{\rm syn,KN} \tag{52}$$

$$\sim 2 \times 10^{-5}(q/30)^{4/3}\frac{L^{1/2}_{B,45}(\mathcal{D}/\Gamma)}{R_{BEL,18}(\Gamma/10)} \quad (\sim 3 \times 10^{15}\,{\rm Hz}\ldots). \tag{53}$$

Hence, sources with $q \gg 1$, $1 < b_{\rm max} < b_{\rm s}$ and power-law electron injection should produce synchrotron 'bumps' peaking in the infrared–ultraviolet (IR–UV) spectral band. The closer a given $b_{\rm max}$ is to $b_{\rm s}$, the more prominent the bump. As discussed, the presence of 'excess' synchrotron emission (the bump) in this case is simply due to KN effects and should not be interpreted as indicating the presence of a new electron acceleration component or a hardening of the low-energy injection spectrum.

We have just estimated the electron injection parameters that would put a luminous blazar into the KN regime studied here. Are there any blazars that actually populate this region of parameter space? Because, for even the brightest blazars, the Energetic Gamma-Ray Experiment Telescope (EGRET) could not detect

gamma-rays much beyond 1 GeV, the extension of the electron energy distribution into KN regime cannot be established using EGRET data. However, quite significant constraints on the high-energy tails of the electron energy distribution are provided by observations of their synchrotron spectra. In the study of Padovani et al. (2003), about half of the objects in their sample of powerful blazar objects have synchrotron spectra peaking at $\nu > 3 \times 10^{13}$ Hz, which implies $b > 1$. In most cases the spectra steepen in the UV band, indicating an injection function with a cut-off or break at $b \sim$ a few, i.e. KN effects may be moderately important. There are a few of these blazars, though, that have a synchrotron peak clearly located in the UV to soft X-ray band and may have $b_{\rm max} \gg 1$. For these objects, assuming the external BEL radiation field is dominant with the characteristics described above, we then predict a high-energy spectral break of the IC component at $\epsilon_{\rm IC,s} \sim 30$ GeV, independent of the observed synchrotron cut-off energy (i.e. $b_{\rm max}$) provided that it is sufficiently large. If the electron injection spectrum for these objects is not unusually soft, i.e. we have $p \lesssim 3$, then as shown in Figs 6–8, for example, a significant fraction of their bolometric luminosity actually emerges in the synchrotron component. In particular, their IC luminosity should be comparable to their synchrotron luminosity, i.e. they would not be gamma-ray loud objects (with $L_{\rm IC}/L_{\rm syn} \gg 1$).

It would be very convenient if powerful blazars had gamma-ray spectra extending to TeV energies, e.g. they would provide very bright sources that could be used to constrain the intensity of the extragalactic background light via the absorption of their gamma-rays (Coppi & Aharonian 1999). Unfortunately, for the BEL parameters we have used, this is impossible unless q is extremely (and implausibly) large. One caveat to this conclusion is that we have not included SSC effects in our estimates, and because the synchrotron emission is much broader in energy than the BEL one, $\gamma_{\rm s}$ and $\epsilon_{\rm IC,s}$ could move to higher values. Note, though, that ϵ_+, the energy above which pair production on the BEL becomes possible, is only $\simeq$50 GeV. Strong Compton TeV emission therefore seems unlikely unless it occurs far from the BEL region and the typical ambient photon energy is in the near-infrared range. Indeed, so far no single FSRQ has been detected in the TeV band – all TeV detected blazars belong to the lower-luminosity, BL Lac class of objects which have either weak or non-existent BEL regions.

6.2 Micro-blazars?

Only two or three EGRET sources have been identified with micro-quasars (Paredes et al. 2000; Combi et al. 2004; Massi et al. 2004). The fact that these objects are HMXB systems containing massive and very luminous companion stars strongly suggests a Compton origin for their gamma-rays. As in blazars, the EGRET observations unfortunately do not provide constraints on $\gamma_{\rm max}$ for these objects. Furthermore, because these sources are relatively weak and completely dominated in the optical/UV band by radiation from the companion stars, their synchrotron component cannot be identified. However, GRS 1915+105 proves that X-ray binaries (XRBs) have the ability to produce much more powerful and relativistic jets (Fender & Belloni 2004) than in the sources just mentioned. If such a powerful jet were to occur in an HMXB and it pointed toward us, we would see a micro-blazar, with relativistically boosted non-thermal radiation dominating over all spectral bands (Georganopoulos, Aharonian & Kirk 2002). Because the spectra of HMXB companion stars peak at $\sim$10 eV, the same value for the BEL in quasars, the values of $\gamma_{\rm KN}$ and $\gamma_{\rm s}$, and of $\epsilon_{\rm IC,KN}$ and $\epsilon_{\rm IC,s}$ are of the same order as for blazars and, therefore, like blazars, they are expected to be GeV emitters and not strong TeV emitters. Due to the much stronger magnetic fields in micro-quasar jets, the synchrotron spectral bumps, produced if $b_{\rm max} \gg 1$, are predicted to peak in the UV/soft X-ray band. Hence, if some of the ultra-luminous X-ray (ULX) sources are in fact micro-blazars pointed at us, they should be strong gamma-ray emitters (Georganopoulos et al. 2002).

However, we must remember that very large q is available only on size scales comparable to those of the binary system. For electron acceleration occurring well down the jet, outside the binary system, the companion star radiation chases the relativistically moving emission region from behind and its energy density is thus Doppler deboosted when viewed in the jet frame. The energy density of the companion star radiation field will be further reduced by the usual factor, $\propto 1/r^2$ where r is the distance from the binary, but this effect can be cancelled out by the fact that the magnetic field energy in a conically expanding jet also drops as $1/r^2$. Closer in to the central object, jets typically have much stronger magnetic fields and, therefore, synchrotron radiation will dominate electron energy losses, even in the Thomson regime. In this case the IC spectrum is expected to break at $\epsilon_{\rm IC,KN}$, i.e. $\sim$1 GeV. This would be the case if, as in blazars, the jet energy is dissipated at 10^{3-4} $(r/r_{\rm g})$, where $r_{\rm g}$ is the gravitational radius of the compact object, i.e. on scales 10^3 times smaller than the typical size of an XRB system.

It should be noted that because the radiation field of the companion star is not symmetric about the jet axis, detailed computations of the non-thermal spectra from XRBs require the integration of emissivities given by equation (15) over the energy distribution of the external radiation field, taking into account that in the source comoving frame, the radiation is boosted by a Doppler factor that depends on the direction of the incoming photons (Khangulian & Aharonian 2005). In other words, the exact geometry of the system is important.

6.3 Pulsars in high-mass X-ray binaries

PSR B1259–63 and PSR J0045–73 provide examples of non-accreting binary pulsars with massive companions (Johnston et al. 1992; Kaspi et al. 1994). Additionally, PSR B1259–63 was recently identified as a TeV source (Aharonian et al. 2005). Ball & Kirk (2000) envisaged two scenarios for production of high-energy radiation in such systems: Comptonization of the radiation field of the companion luminous star directly by the pulsar ultrarelativistic wind (i.e. a bulk Compton scenario) or by particles accelerated in the terminal wind shock formed due to the confinement of the pulsar wind by the wind from the companion star. Because for finite values of $q \gg 1$, the IC spectrum has a high-energy break at $\epsilon_{\rm IC,br} = \min(\epsilon_{\rm IC,s}, \epsilon_{\rm IC,max})$, the condition for efficient TeV production is $\epsilon_{\rm IC,s} \geqslant 10^6$ and $\epsilon_{\rm IC,max} \geqslant 10^6$. Because $\epsilon_{\rm IC,s} \sim \gamma_{\rm s} b_{\rm s} \gamma_{\rm KN}$, where $\gamma_{\rm KN} = 1/(4\epsilon_0) \sim 10^4$, this translates into the condition $b_{\rm s} > 100$, i.e. for a mono-energetic field, we again need a very large $q \gtrsim 10^3$. In the shocked wind scenario, this condition provides an upper limit on the strength of the magnetic field in the shocked plasma. In the bulk Compton scenario, the condition is satisfied even for strongly magnetized winds. This is because electrons are cold and frozen to the magnetic field lines. Hence, their energy losses via the synchrotron mechanism are negligible and, effectively, the value of q is infinite. Of course, to reach TeV energies in this scenario, the bulk Lorentz factor of the wind is required to be of the order of 10^6, which is consistent with estimations of the wind speed in the Crab nebula (Rees & Gunn 1974).

6.4 Kiloparsec-scale jets

Jets in quasars encounter a variety of radiation fields as they make their way out from the central black hole, starting from the radiation field of the black hole accretion disc and ending with the CMB. For jets that are relativistic from the start, the largest q would be reached near the base of the jet. The lack of bulk Compton features in the soft X-ray band suggests this is not the case (Moderski et al. 2004), and thus that the energetically dominant Compton interactions of a jet with external radiation field seem to take place not earlier than in the BEL region, i.e. around 0.1–1 parsec from the centre. Large values of q are also expected in sources triggered at 1–10 parsec distances where the diffuse component of the external field is likely dominated by the thermal emission from hot dust (Sikora et al. 2002). At progressively larger distances, the jet undergoes Compton interactions with narrow emission lines, with stellar radiation, and finally the CMB. As of now there is no direct evidence that at such distances electrons are injected with $b_{\rm max} \gg 1$, but this may simply be due to the sensitivity and angular resolution of present gamma-ray detectors. Indirect evidence in favour of $b_{\rm max} \gg 1$ and $q \gg 1$ for kpc-scale jets may come from the work of Dermer & Atoyan (2002). They argued that a purely synchrotron emission model, with a jet magnetic energy density less than the CMB energy density, can successfully explain not just the observed radio-to-optical jet radiation, but also the X-ray flux detected by *Chandra*, despite the fact that the *Chandra* flux often lies above an extrapolation of the radio–optical spectrum. This is achieved by the formation of a synchrotron bump above $\epsilon_{\rm syn,KN}$ due to the KN effects we have described here. We note, however, that this particular model requires extremely large $\gamma_{\rm max}$, at least one order of magnitude larger than $\gamma_{\rm KN} = 1/(4\Gamma\epsilon_{\rm CMB}) \simeq 2 \times 10^7/(\Gamma/10)(1+z)$, where $\epsilon_{\rm CMB}$ $(z=0) \sim 10^{-9}$.

7 CONCLUSIONS

We have studied, both analytically and using accurate numerical codes, the electromagnetic spectra produced by relativistic electrons in a magnetized non-thermal source that is immersed in a dense radiation field originating outside the source. We consider the case when the steady-state electron energy distribution is determined by the injection energy spectrum of the accelerated electrons and their energy losses, dominated by synchrotron radiation and Compton scattering which may extend deeply into the KN regime. We concentrate on the poorly studied region of parameter space in which the energy density of the radiation field inside the source exceeds that of the magnetic field, i.e. values of the parameter $q = u_0/u_B > 1$. Fig. 10 summarizes the three main regions we find for the overall parameter space for our problem.

(i) In zone I ($q < 1$), the electron distribution is determined by synchrotron cooling and KN effects do not appear in the synchrotron spectrum. The Compton spectrum, however, shows a strong break at $\epsilon_{\rm IC,KN}$ due to the strong KN reduction in the Compton scattering rate that starts for electron energies $\gamma > \gamma_{\rm KN}$. Assuming the maximum electron acceleration energy, $\gamma_{\rm max}$, is sufficiently large that $\epsilon_{\rm IC,max} > \epsilon_{\rm IC,KN}$, the position of this break is independent of $\gamma_{\rm max}$. In zone Ib ($1 < q \lesssim 3$), we start to see a hardening of the electron distribution that is reflected in the synchrotron emission spectrum. The hardening occurs because Compton cooling is now an important contribution to the total electron cooling rate, and Compton losses decrease at high energies due to the KN effect. The effect is not large, however. The Compton spectrum does not show significant differences because synchrotron losses start to dominate again at $\gamma_{\rm s} < \gamma_{\rm KN}$.

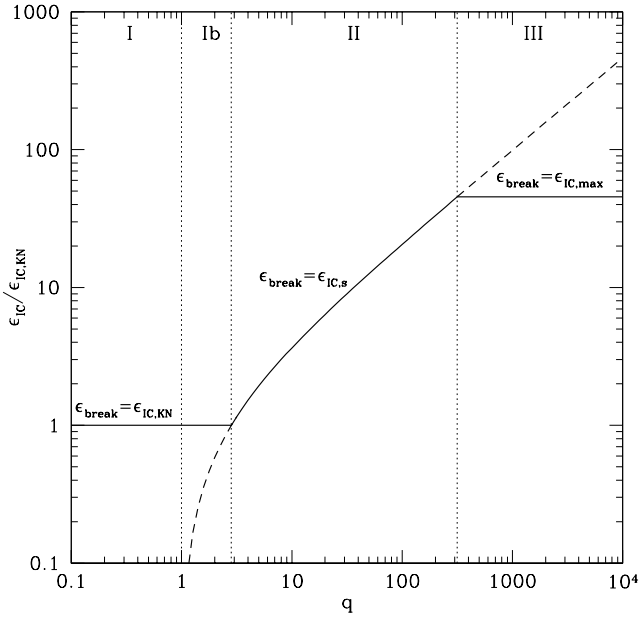

Figure 10. Schematic illustration showing the location of the high-energy break in the Compton spectra as a function of q. (For details, see text.)

(ii) In zones II and III, $q \gg 1$, and the distortion in the electron distribution due to the reduction in Compton cooling is very large. The synchrotron spectrum correspondingly shows a strong, hard excess over the Thomson limit asymptote. The Compton spectrum below $\epsilon_{\rm IC,s}$, however, does not show a strong deviation from the low-energy Thomson limit because the KN decline in the Compton rate is compensated by the corresponding increase in the electron density. The distinction between zones II and III is that in zone II, the maximum electron energy is such that $\gamma_{\rm max} > \gamma_{\rm s}$. Above $\gamma_{\rm s}$ synchrotron cooling dominates. The energy distributions of the electrons and the synchrotron radiation reach asymptotes with the same slopes as in the Thomson regime but with amplitudes enhanced by a factor q. The Compton spectrum, on the other hand, shows a strong break at $\epsilon_{\rm IC,s}$ because the KN reduction in the scattering is no longer compensated by a hardening of the electron energy distribution. In zone II, then, the Compton spectrum breaks at an energy independent of $\gamma_{\rm max}$. In zone III, instead, the synchrotron losses never dominate, and the location of the Compton high-energy break is determined by the maximum electron energy just as it is for the synchrotron component. The combination of the high-energy break and the hardening of the synchrotron spectrum at lower energies leads to the formation of a strong synchrotron bump.

The specific conclusions of our study are as follows.

(i) The IC spectra have high-energy breaks at $\epsilon_{\rm IC,max}$, if $b_{\rm max} < b_{\rm s}$, or at $\epsilon_{\rm IC,s}$, if $b_{\rm max} > b_{\rm s}$. The former is related to the high-energy cut-off of the electron injection function, and the latter to the strong steepening of the IC spectrum, caused by domination of energy losses of electrons with $\gamma > \gamma_{\rm s}$ by synchrotron mechanism.

(ii) Synchrotron spectra undergo strong hardening at $\epsilon > \epsilon_{\rm syn,KN}$, with $|\Delta\alpha|$ reaching $\sim$0.5–0.75 for $q > 30$. Hence, for very hard electron injection spectra, with $p < 1$, the spectral index α $(=0.5 - |\Delta\alpha|)$ can even reach negative values. The hardening is visible already at $\epsilon \simeq 0.1\epsilon_{\rm syn,KN}$.

(iii) For $1 < b_{\rm max} \leqslant b_{\rm s}$, the hardening of the synchrotron spectrum combined with the high-energy break at $\epsilon_{\rm s,max}$ leads to the formation of a 'bump' in the high-energy portion of the synchrotron spectrum.

For $b_{\max} \gg b_s$, the hardening of the synchrotron spectrum stops at $\epsilon_{\rm syn,s}$ and the spectrum continues with the same slope as in the Thomson regime but with a normalization q times larger.

(iv) For hard electron injection functions ($p < 2$) and $b_{\max} > b_s$, the luminosity of the synchrotron component is larger than the luminosity of the IC component, even for $q \gg 1$. This is because for a hard injection function most of the power is supplied to electrons with $\gamma > \gamma_s$, and the energy losses for these electrons are dominated by synchrotron radiation. For $p = 2$ the luminosities of the synchrotron and IC spectral peaks are of the same order.

(v) When KN effects are important, both the IC and especially the synchrotron component can have spectra harder than the hardest spectrum possible in the Thomson limit for fast cooling electrons ($\alpha = 0.5$).

(vi) Generally, photon–photon pair production of the Compton gamma-rays on the ambient radiation field may be important for $\gamma_{\max} \gg \gamma_{\rm KN}$. However, for a pair production energy threshold exceeding $\epsilon_{\rm IC,s}$, the fraction of the gamma-ray luminosity converted into pairs is not significant, even if the opacity for pair production is large.

(vii) The continuous energy loss approximation for the evolution of the electron distribution appears to work reasonably well, even for $\gamma_{\max} \gg \gamma_{\rm KN}$. Use of this approximation can save considerable computing time.

(viii) The KN effects we have discussed can be important in powerful blazars and HMXBs, with the latter including accreting compacts objects and rotationally powered pulsars.

ACKNOWLEDGMENTS

This project was partially supported by Polish KBN grants 1 P03D 00928, PBZ-KBN-054/P03/2001 and by the Department of Energy contract to SLAC no. DE-AC3-76SF00515. MS and PC thank the Fellows of the MPI für Kernphysik, and SLAC and KIPAC for their hospitality and support during their stays there. PC was also supported in part by a Yale University Senior Faculty Fellowship.

REFERENCES

Aharonian F. A., Atoyan A. M., 1981, Ap&SS, 79, 321
Aharonian F. A. et al. 2005, A&A, preprint (doi: 10.1051/0004-6361: 20052983)
Ball L., Kirk J. G., 2000, Astropart. Phys., 12, 335
Blumenthal G. R., Gould R. J., 1970, Rev. Mod. Phys., 42, 237
Combi J. A., Ribó M., Mirabel I. F., Sugizaki M., 2004, A&A, 422, 1031
Coppi P. S., 1992, MNRAS, 258, 657
Coppi P. S., Aharonian F. A., 1999, Astropart. Phys., 11, 35
Coppi P. S., Blandford R. D., 1990, MNRAS, 245, 453
Dermer C. D., Atoyan A. M., 2002, ApJ, 568, L81
Felten J. E., Morrison P., 1966, ApJ, 146, 686
Fender R., Belloni T., 2004, ARA&A, 42, 317
Georganopoulos M., Aharonian F. A., Kirk J. G., 2002, A&A, 388, L25
Johnston S., Manchester R. N., Lyne A. G., Bailes M., Kaspi, V. M., Qiao G., D'Amico N., 1992, ApJ, 387, L37
Jones F. C., 1968, Phys. Rev., 167, 1159
Kaspi V. M., Johnston S., Bell J. F., Manchester R. N., Bailes M., Bessell M., Lyne A. G., D'Amico N., 1994, ApJ, 423, L43
Khangulian D., Aharonian F. A., 2005, in Aharonian F. A., Völk H. J., Horns D., eds, AIP Conf. Proc. 745, High Energy Gamma-Ray Astronomy. American Institute of Physics, New York, p. 359
Kusunose M., Takahara F., 2005, ApJ, 621, 285
Kusunose M., Takahara F., Kato T., 2004, Prog. Theor. Phys. Suppl., 155, 367
Massi M., Ribó M., Paredes J. M., Garrington S. T., Peracaula M., Martí J., 2004, A&A, 414, L1
Moderski R., Sikora M., Madejski G. M., Kamae T., 2004, ApJ, 611, 770
Mukherjee R. et al., 1997, ApJ, 490, 116
Padovani P., Perlman E. S., Landt H., Giommi P., Perri M., 2003, ApJ, 588, 128
Paredes J. M., Martí J., Ribó M., Massi M., 2000, Sci, 288, 2340
Ravasio M., Tagliaferri G., Ghisellini G., Tavecchio F., Böttcher M., Sikora M., 2003, A&A, 408, 479
Rees M. J., Gunn J. E., 1974, MNRAS, 167, 1
Sikora M., Błażejowski M., Moderski R., Madejski G. M., 2002, ApJ, 577, 78
von Montigny C. et al., 1995, ApJ, 440, 525
Zdziarski A. A., 1988, ApJ, 335, 786
Zdziarski A. A., 1989, ApJ, 342, 1108
Zdziarski A. A., Krolik J. H., 1993, ApJ, 409, L33

APPENDIX A: SCATTERING OF DIRECTED PHOTON BEAMS ON ISOTROPICALLY DISTRIBUTED RELATIVISTIC ELECTRONS

The general formula for the distribution in energy and angle of the scattered photons per electron per unit time for the photon beams is given by equation (14) in Aharonian & Atoyan (1981). For $\epsilon \gg \epsilon_0$ and $\gamma \gg 1$, this formula takes the form (see equations 20 and 21 in Aharonian & Atoyan 1981)

$$\frac{\partial \dot{N}_{\rm sc}(\epsilon,\gamma,\theta)}{\partial\epsilon\partial\Omega} \simeq \frac{3}{16\pi} c\sigma_{\rm T} \int_{\epsilon_{0,m}(\gamma,\theta)} \frac{n_{\epsilon_0}}{\epsilon_0\gamma^2} f(\epsilon,\epsilon_0,\gamma,\theta)\,{\rm d}\epsilon_0, \qquad \text{(A1)}$$

where ϵ_0 and ϵ are energies of the incident and scattered photons in $m_{\rm e}c^2$ units, respectively, θ is the scattering angle, n_{ε_0} is the photon number density per energy,

$$\epsilon_{0,m}(\gamma,\theta) = \frac{\epsilon}{2(1-\cos\theta)\gamma^2[1-(\epsilon/\gamma)]}, \qquad \text{(A2)}$$

and

$$f(\epsilon,\epsilon_0,\gamma,\theta) = 1 + \frac{w^2}{2(1-w)} - \frac{2w}{b_\theta(1-w)} + \frac{2w^2}{b_\theta^2(1-w)^2}, \qquad \text{(A3)}$$

where $b_\theta = 2(1-\cos\theta)\epsilon_0\gamma$, and $w = \epsilon/\gamma$.

APPENDIX B: SCATTERING OF ISOTROPICALLY DISTRIBUTED PHOTONS ON ISOTROPICALLY DISTRIBUTED RELATIVISTIC ELECTRONS

For an isotropic radiation field

$$\frac{\partial \dot{N}_{\rm sc}(\epsilon,\gamma)}{\partial\epsilon\partial\Omega} = \frac{1}{4\pi}\frac{\partial \dot{N}_{\rm sc}(\epsilon,\gamma)}{\partial\epsilon} = \frac{3}{16\pi} c\sigma_{\rm T} \int_{\epsilon_{0,m}(\gamma)} \frac{n_{\epsilon_0}}{\epsilon_0\gamma^2} f_{\rm iso}(\epsilon,\epsilon_0,\gamma)\,{\rm d}\epsilon_0, \qquad \text{(B1)}$$

where (see equation 23 in Aharonian & Atoyan 1981)

$$\epsilon_{0,m}(\gamma) = \frac{\epsilon}{4\gamma^2[1-(\epsilon/\gamma)]}, \qquad \text{(B2)}$$

and

$$f_{\rm iso}(\epsilon,\epsilon_0,\gamma) = \frac{1}{4\pi}\int_{\theta_{\min}} f(\epsilon,\epsilon_0,\gamma,\theta)\,{\rm d}\Omega = \frac{1}{2}\int^{\cos\theta_{\min}} f(\epsilon,\epsilon_0,\gamma,\theta)\,{\rm d}\cos\theta, \qquad \text{(B3)}$$

where $\cos\theta_{\rm min} = 1 - 2w/[b(1-w)]$. Integration in equation (B3) can be performed analytically giving (see equation 22 in Aharonian & Atoyan 1981)

$$f_{\rm iso}(\epsilon, \epsilon_0, \gamma) = 1 + \frac{w^2}{2(1-w)} + \frac{w}{\tilde{b}(1-w)} - \frac{2w^2}{\tilde{b}^2(1-w)^2} - \frac{w^3}{2\tilde{b}(1-w)^2} - \frac{2w}{\tilde{b}(1-w)} \ln\frac{\tilde{b}(1-w)}{w}, \quad \text{(B4)}$$

where $\tilde{b} = 4\epsilon_0\gamma$. Note that $f_{\rm iso}$ is fully equivalent to the term bracketed in equation (9) in Jones (1968).

APPENDIX C: ELECTRON ENERGY LOSSES

The rate of IC energy losses of electrons is

$$|\dot{\gamma}|_{\rm IC} \simeq \frac{3}{4} c\sigma_{\rm T} \frac{1}{\gamma^2} \int \frac{n_{\epsilon_0}}{\epsilon_0} \left[\int f_{\rm iso}(\epsilon, \epsilon_0, \gamma)\epsilon \, {\rm d}\epsilon \right] {\rm d}\epsilon_0. \quad \text{(C1)}$$

The inner integral has an analytical solution (see equation 46 in Jones 1968)

$$\int f_{\rm iso}(\epsilon, \epsilon_0, \gamma)\epsilon {\rm d}\epsilon = \frac{\gamma^2 g(\tilde{b})}{\tilde{b}}, \quad \text{(C2)}$$

where

$$g(\tilde{b}) = \left(\frac{1}{2}\tilde{b} + 6 + \frac{6}{\tilde{b}}\right) \ln(1+\tilde{b}) - \left(\frac{11}{12}\tilde{b}^3 + 6\tilde{b}^2 + 9\tilde{b} + 4\right) \times \frac{1}{(1+\tilde{b})^2} - 2 + 2{\rm Li}_2(-\tilde{b}) \quad \text{(C3)}$$

and $\rm Li_{\,2}$ is the dilogarithm. Hence,

$$|\dot{\gamma}|_{\rm IC} = \frac{4c\sigma_{\rm T}}{3} \gamma^2 \int f_{\rm KN}(\tilde{b})\epsilon_0 n_{\epsilon_0} \, {\rm d}\epsilon_0, \quad \text{(C4)}$$

where

$$f_{\rm KN}(\tilde{b}) = 9g(\tilde{b})/\tilde{b}^3. \quad \text{(C5)}$$

This paper has been typeset from a TEX/LATEX file prepared by the author.